applied optics

Multiple beam interference model for measuring parameters of a capillary

Qiwei Xu,[1] Wenjing Tian,[1] Zhihong You,[3] and Jinghua Xiao[1,2,*]

[1]School of Science, Beijing University of Posts and Telecommunications, Beijing 100876, China
[2]State Key Laboratory of Information Photonics and Optical Communications, Beijing University of Posts and Telecommunications, Beijing 100876, China
[3]Department of Physics, Beijing Normal University, Beijing 100875, China
*Corresponding author: jhxiao@bupt.edu.cn

Received 11 May 2015; revised 6 July 2015; accepted 10 July 2015; posted 13 July 2015 (Doc. ID 240532); published 31 July 2015

A multiple beam interference model based on the ray tracing method and interference theory is built to analyze the interference patterns of a capillary tube filled with a liquid. The relations between the angular widths of the interference fringes and the parameters of both the capillary and liquid are derived. Based on these relations, an approach is proposed to simultaneously determine four parameters of the capillary, i.e., the inner and outer radii of the capillary, the refractive indices of the liquid, and the wall material. © 2015 Optical Society of America

OCIS codes: (120.0120) Instrumentation, measurement, and metrology; (120.3180) Interferometry; (120.2650) Fringe analysis; (290.0290) Scattering; (290.3030) Index measurements.

http://dx.doi.org/10.1364/AO.54.006948

1. INTRODUCTION

Refractive index (RI) of liquid is a key parameter in physics, chemistry, and biology. Thus, its precise measurement is of great significance. In the last few years, several methods have been proposed to measure the RI of liquid by using a capillary. A typical example is the capillary interferometry [1–12], where the RI of the liquid can be obtained by measuring the interference fringes. However, the capillary interferometry is still a little complicated, in both experiment and theoretical analysis. Treating the capillary as an interferometer as well, Hou *et al.* [13] propose a simpler method based on dual-beam interference. They blacked the inner wall of the tube with ink, and analyzed the interference fringes produced by two lights that differ in their paths, one passes through the capillary wall, and the other is reflected by the surface of the capillary. They derived the spacing of fringes at a certain location on the screen as a function of the capillary parameters, which was then used to determine the outer radius of the capillary if the RI of the capillary is known, and vice versa. On the other hand, You *et al.* [14,15] focused on the global structure of emergent light from the capillary based on geometrical optics. It was found that by a simple measurement of the deviation angles of several intensity step points, the RIs of both the liquid and the capillary wall, as well as the ratio of the capillary radius can be obtained. A difficulty of the You *et al.* method is the localization of the step points, because these step points are not strictly points as suggested by the geometrical optics. Instead, these spots have certain span widths because of the wave nature of light, which brings error to the measurement, and this disadvantage become obvious when we use a thin capillary.

In this paper, a method is proposed that can accurately and simultaneously measure four parameters, i.e., RIs of the liquid and the capillary wall, inner and outer radii of the capillary, based on a multiple beam interference model. We employ ray tracing method [16,17] and interference theory to analyze the interference patterns of a capillary filled with transparent liquid. The emergent lights are classified into rays 1–7 in accordance with their paths. By tracing the paths of these rays, one obtains the intensities of these rays. Different rays incident on the same spot of the screen will interfere. The interference patterns can be calculated according to the phase differences of these rays. We find that in most cases, usually only two or three of these rays are dominant contributors to the interference pattern at a specific deviation angle while other rays can be ignored. Different combinations of dominant rays give rise to different patterns. To be specific, a dual-beam interference results in periodic stripes, while the interference of three rays produces envelope fringes. The angular widths of the fringes are also obtained, which are well related to the parameters of the capillary and the liquid. Based on this relation, a simple method is developed to simultaneously measure RIs of the liquid and the capillary wall, inner and outer radii of the capillary. To determine the error of this method, we build an experiment to measure these parameters. First, we generate interference patterns for a certain set of parameters. Then we *measure* the angular widths of these simulated fringes and determine the

parameters by using the proposed method. The error of the method is proved to be less than 0.03% in theory. We also conducted a practical experiment, from which the errors of the parameter were found to be of 0.1% order, and the error source is analyzed.

The rest of the paper is organized as follows. In Section 2, the experimental phenomena are introduced. In Section 3, the ray tracing method and interference theory are used to analyze the intensity distribution and interference patterns, respectively. The method to measure parameters is proposed in Section 4. Finally, in Section 5, we draw our conclusions.

2. EXPERIMENTAL INTERFERENCE PATTERNS

The experimental setup is shown in Fig. 1. A capillary filled with transparent liquid is placed vertically, 2 m away from a He–Ne laser (wavelength of 632.8 nm). A rotating screen is placed with a radius about 1 meter. The RI of the capillary wall is $n_0 = 1.4710$ [14], and the liquid inside the capillary is phenylethyl alcohol, with a RI $n = 1.5323$. The RI of the liquid is obtained from an Abbe refractometer. The inner and outer radii of the capillary are, respectively, $r = 0.256$ mm and $R = 0.505$ mm, measured by a reading microscope (JCD3). Since the diameter of the incident beam (9 mm) is much larger than that of the capillary (1.010 mm), the laser beam can be regarded as a plane wave.

The typical interference fringes are presented in Fig. 2. The interference patterns can be divided into three classes. The first class is simple periodic fringes [like A and C in Figs. 2(b)] similar to those of the double-slit interference. Those contain fine structure in the pattern (envelopes), like B in Fig. 2(b) are classified into the second class; while the third class are complicated irregular stripes like D and E in Fig. 2(b). In the following sections, we focus on patterns of class 1 and 2.

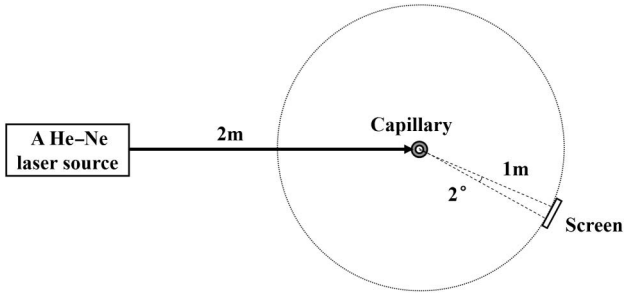

Fig. 1. Experimental setup to observe interference patterns around the capillary.

3. THEORETICAL ANALYSIS

Two classes of regular patterns have been shown in Fig. 2. To analyze these patterns, we need to combine the theories of geometrical optics and wave optics. For a capillary filled with transparent liquid, the process of interference is subtle and complicated. Thus, we employ a multibeam interference model to analyze these patterns.

A. Intensity Distribution of Different Rays

It can be derived from Fresnel's Law that the reflectivity of both interfaces, i.e., the air-capillary interface and the capillary-liquid interface, are very low. Hence, it suffices to consider only the lights that are reflected no more than one time. The emergent lights can be classified into rays 1–7 according to their paths, as shown in Fig. 3. Because of symmetry, only the upper half of incident lights are taken into account. The angle of incidence, denoted by θ, is defined as the angle between the incident light and the normal to the surface of the capillary. Meanwhile, the deviation angle β is defined as the angle from the incident light to the emergent light with positive sign in the clockwise sense.

The deviation for the angles of seven rays can be obtained by employing the three laws of the geometrical optics, which are

$$\beta_1 = 2\theta - \pi \left[0 \le \theta \le \frac{\pi}{2}\right], \tag{1a}$$

$$\beta_2 = 2(\theta - \varphi + \delta) - \pi \left[0 \le \theta \le \arcsin\frac{rn_0}{R}\right], \tag{1b}$$

$$\beta_3 = 2(\theta - \varphi + \delta - 2\alpha) + \pi \left[0 \le \theta \le \arcsin\frac{rn_0}{R}\right], \tag{1c}$$

$$\beta_4 = 2(\theta - 2\varphi + 2\delta - 2\alpha) + \pi \left[0 \le \theta \le \arcsin\frac{rn_0}{R}\right], \tag{1d}$$

$$\beta_5 = 2(\theta - 2\varphi) + \pi \left[\arcsin\frac{rn_0}{R} \le \theta \le \frac{\pi}{2}\right], \tag{1e}$$

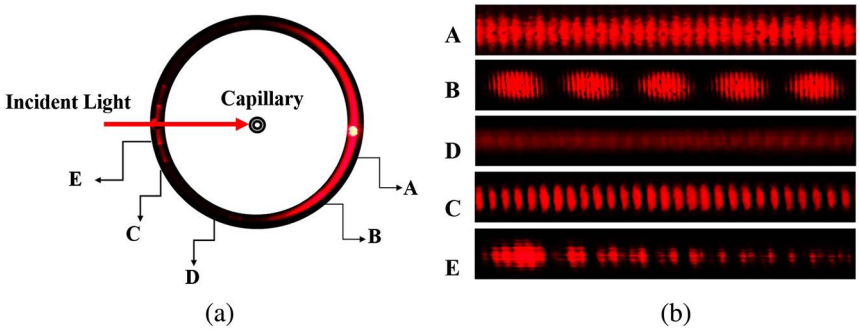

Fig. 2. Interference patterns in the experiment. Parameters are $n_0 = 1.4710$, $R = 0.505$ mm, $r = 0.256$ mm, $n = 1.5323$. A–E in (b) show the detailed patterns at different angles, with an angular width of about 2°, and the center angles are about 10, 40, 90, 160, and 170°, respectively. A–E in (b) are located, respectively, in A–E in (a).

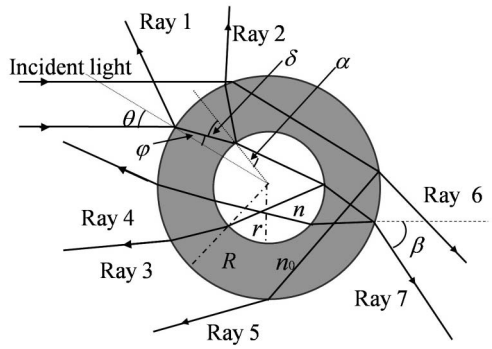

Fig. 3. Paths of rays 1–7. Rays 1 and 2 are reflected on the outer and inner convex interfaces, respectively. Ray 3 is reflected by the inner concave wall. Rays 4 and 5 are reflected by the outer-convex wall, while ray 4 passes through the liquid, and ray 5 does not. Rays 6 and 7 are refractive lights which pass through the capillary wall and the liquid, respectively.

$$\beta_6 = 2(\theta - \varphi)\left[\arcsin\ \frac{rn_0}{R} \le \theta \le \frac{\pi}{2}\right], \tag{1f}$$

$$\beta_7 = 2(\theta - \varphi + \delta - \alpha)\left[0 \le \theta \le \arcsin\ \frac{rn_0}{R}\right]. \tag{1g}$$

Note that when the incident angle θ is arcsin (rn_0/R), the refractive ray is tangent to the inner wall of the capillary. Note that RI of the liquid is greater than that of capillary wall $(n > n_0)$ in this paper.

The intensity distributions of the seven rays can be determined by taking into account the reflectance and transmittance at each interface that the rays pass through. Let the intensity of incident lights be I_0, and the intensity of emergent ray i be $I_i(\beta_i)$, we have

$$I_i(\beta_i) = I_0 S_i(\theta, \beta_i), \tag{2}$$

where $S_i(\theta, \beta_i)$ is called the scattering factor of ray i, which is the product of transmittance and reflectance at either inner or outer capillary wall. For example, ray 5 is successively refracted, reflected, and then refracted again. If the angles of incidence at each interface are θ and φ, then $S_5(\theta, \beta_5)$ is given by

$$S_5(\theta, \beta_5) = T(\theta) R_e(\varphi) T(\varphi), \tag{3}$$

where reflectance (R_e) and transmittance (T) are [18]

$$R_e(\gamma) = \left[\frac{\sin(\gamma - \gamma_1)}{\sin(\gamma + \gamma_1)}\right]^2, \tag{4}$$

$$T(\gamma) = 1 - R_e(\gamma). \tag{5}$$

In Eq. (4), γ and γ_1 are the angles of incidence and refraction, respectively. The scattering factors for other rays can be calculated in the same way. Hence, we can obtain the intensity distributions of emergent lights for all rays, as shown in Fig. 4. Note that Fig. 4 only shows the intensity distribution of emergent light in the range of 0°–180°.

Obviously, different rays are reflected and refracted at different places on the screen, and the deviation angle can be further divided into five regions (A–E). Irregular fringes of class 3 appears in regions D, E, thus we focus on regions A–C in the rest

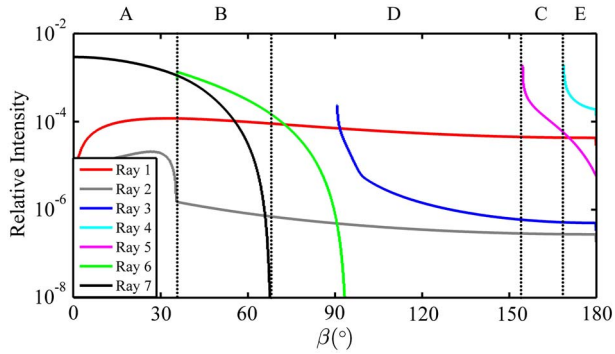

Fig. 4. Intensity distributions for seven rays in five angular regions A–E.

of the paper. Meanwhile, according to Fig. 4, intensities of rays on the boundary between adjacent regions are unstable, causing irregular patterns, and the block part of regions A, B, and C are analyzed. From Fig. 4, it is easy to conclude that the relative intensity of the seven rays differ so much that only two or three rays (high intensity) contribute to the interference pattern at a certain angular region, while other rays (low intensity) can be ignored, as listed in Table 1. Note that intensity of ray 2 is small at all angles, so it is not listed in the table.

The intensity distributions of different rays are obtained by using the ray tracing method. Since a coherent beam of light is incident on the capillary, the emergent lights of different rays that arrive at the same spot of the screen can interfere with each other and produce the various patterns shown in Fig. 2(b).

B. Analysis of Interference Patterns

Since the intensities of the seven rays are known, their phase must be determined to obtain the interference patterns in each region.

It can be learned from Table 1 that rays 1, 7, and rays 1, 5, and rays 1, 6, and 7 contribute to the interference fringes in regions A, C, and B, respectively. The intensities of the interference patterns in A, C, and B are [19]

$$I_A = A_1^2 + A_7^2 + 2A_1A_7 \cos\left[\frac{2\pi(L_7 - L_1)}{\lambda}\right], \tag{6}$$

$$I_C = A_1^2 + A_5^2 + 2A_1A_5 \cos\left[\frac{2\pi(L_5 - L_1)}{\lambda}\right], \tag{7}$$

Table 1. Three Different Angular Regions with Different Combination of Rays[a]

	Ray 1	Ray 3	Ray 4	Ray 5	Ray 6	Ray 7
A (0°–36°)	✓					✓
B (36°–67°)	✓				✓	✓
C (154°–168°)	✓	(Ignored)		✓		

[a]Rays with much smaller intensity are ignored compared with others in the same region.

$$I_B = A_1^2 + A_6^2 + A_7^2 + 2A_1A_6\cos\left[\frac{2\pi(L_6 - L_1)}{\lambda}\right] + 2A_1A_7\cos\left[\frac{2\pi(L_7 - L_1)}{\lambda}\right] + 2A_6A_7\cos\left[\frac{2\pi(L_6 - L_7)}{\lambda}\right]. \quad (8)$$

Here, λ is the wavelength of the laser, $A_i(\beta) = [I_i(\beta)]^{1/2}$ is the amplitude of the electromagnetic field of ray i. To calculate the phase of these rays, two lines are set as the starting and ending of phase calculation, as shown in Fig. 5. The optical path length of rays 1, 5, 6, and 7 from line 1 to line 2 are

$$L_1 = 2R(1 - \cos\theta), \quad (9)$$

$$L_5 = 2R(1 - \cos\theta) + 4n_0R\cos\varphi, \quad (10)$$

$$L_6 = 2R(1 - \cos\theta) + 2n_0R\cos\varphi, \quad (11)$$

$$L_7 = 2R(1 - \cos\theta) + 2n_0R\cos\varphi - 2n_0r\cos\delta + 2nr\cos\alpha. \quad (12)$$

We calculate the interference fringes in regions A, B, and C according to Eq. (6) to Eq. (12), and the results are shown in Figs. 6(b), 6(d), and 6(f), together with the experimental phenomena [Figs. 6(a), 6(c), and 6(e)]. The simulations are seen to be in good agreement with the experimental results.

A brief analysis of these patterns is given as follows. We define $\delta_{51} = 2\pi(L_5 - L_1)/\lambda$, $\delta_{61} = 2\pi(L_6 - L_1)/\lambda$, $\delta_{71} = 2\pi(L_7 - L_1)/\lambda$, and $\delta_{67} = 2\pi(L_6 - L_7)/\lambda$ as the phase differences between the rays. Note that the angular widths of the interference patterns in Fig. 6 are of the order of 1°; in this small interval, it is reasonable to make two assumptions: (1) A_i ($i = 1, 5, 6, 7$) are constant (Fig. 4); and (2) phase differences grow linearly with β (Fig. 7). Then let $\delta_{51} = k_1\beta + c_1$, $\delta_{61} = k_2\beta + c_2$, $\delta_{71} = k_3\beta + c_3$, and $\delta_{67} = (k_2 - k_3)\beta + c_4$. Here, $c_i (i = 1 \sim 4)$ only influence the position of the patterns, thus we set $c_i = 0$ for simplicity.

Inserting δ_{71} into Eq. (6), we have

$$I_A = A_1^2 + A_7^2 + 2A_1^2A_7^2\cos\delta_{71} = A_1^2 + A_7^2 + 2A_1^2A_7^2\cos(k_3\beta). \quad (13)$$

Similarly, intensity distribution in region C is

$$I_C = A_1^2 + A_5^2 + 2A_1^2A_5^2\cos\delta_{51} = A_1^2 + A_5^2 + 2A_1^2A_5^2\cos(k_1\beta). \quad (14)$$

Since $A_i (i = 1, 5, 7)$ is constant, the intensity distributions in regions A and C are cosine functions of β. Therefore, the patterns in regions A and C are simple periodic stripes. Meanwhile,

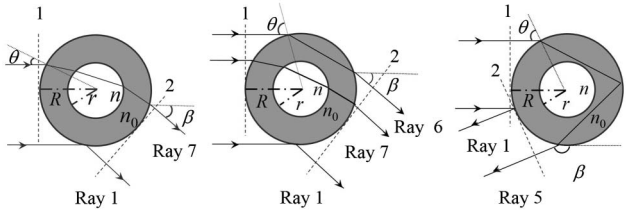

Fig. 5. Multibeam interference of regions: (a) A; (b) C; (c) B.

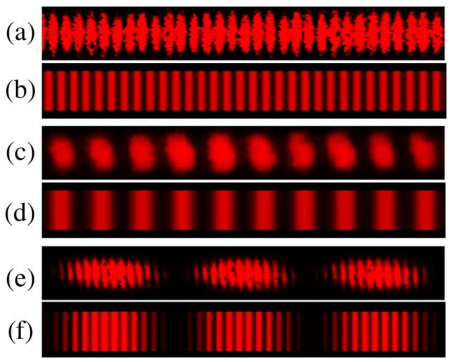

Fig. 6. Experimental patterns and simulations. Parameters are $n_0 = 1.4710$, $R = 0.505$ mm, $r = 0.256$ mm, $n = 1.5323$. The center angles in (a), (c), and (e) are about 5°, 160°, and 40°, corresponding to angular regions A, C, and B, respectively. The angular widths of the photo in (a), (c), and (e) are about 2°, 1.6°, and 1.3°, respectively.

it can be learned from Figs. 7(a) and 7(c) that $k_1 > k_3$, thus the stripes in region C are wider than those in region A.

The interference in region B is more complicated since there are three rays in it. Inserting δ_{61}, δ_{71}, and δ_{67} into Eq. (8), one obtains

$$\begin{aligned} I_B &= A_1^2 + A_6^2 + A_7^2 + 2A_1A_6\cos\delta_{61} + 2A_1A_7\cos\delta_{71} + 2A_6A_7\cos\delta_{67} \\ &= A_1^2 + A_6^2 + A_7^2 + 2A_1A_6\cos(k_2\beta) + 2A_1A_7\cos(k_3\beta) + 2A_6A_7\cos[(k_2 - k_3)\beta] \\ &= A_1^2 + A_6^2 + A_7^2 + 2A_1(A_6 - A_7)\cos(k_2\beta) + 4A_1A_7\cos\left[\frac{(k_2 + k_3)\beta}{2}\right]\cos\left[\frac{(k_2 - k_3)\beta}{2}\right] + 2A_6A_7\cos[(k_2 - k_3)\beta] \\ &= y_0 + y_1 + y_2, \end{aligned} \quad (15)$$

where $y_0 = A_1^2 + A_6^2 + A_7^2 + 2A_1(A_6 - A_7)\cos(k_2\beta)$ and $y_1 = 4A_1A_7\cos[(k_2 + k_3)\beta/2]\cos[(k_2 - k_3)\beta/2]$ and $y_2 = 2A_6A_7\cos[(k_2 - k_3)\beta]$. Note that $A_6 - A_7 \ll A_6(A_7)$, $2A_1(A_6 - A_7)\cos(k_2\beta)$ can be ignored, then y_0 can be regarded as a constant. y_1, y_2 are shown in Fig. 8(a). Since $k_2 \approx k_3$ (Fig. 7(b)), $(k_2 - k_3)/2 \ll (k_2 + k_3)/2$ is valid, thus y_1 describes an envelope pattern with two periods, $4\pi/(k_2 + k_3)$ and $4\pi/(k_2 - k_3)$ as shown in Fig. 8(b). Obviously, y_1 cannot solely produce the beautiful pattern in the experiment [Fig. 6(e)]. From both Eq. (15) and Fig. 8, we see that the maximum and minimum of y_2 [Fig. 8(c)] correspond to that of the envelope of y_1, respectively. Thus, y_2 relatively darkens the obscure part of y_1 and brightens the distinct part of the envelope. Therefore, it is the combination of y_1 and y_2 that produces the elegant "enhanced envelopes" pattern. As a result, the contour of enhanced envelopes is only determined by rays 1 and 7, because its period is $4\pi/(k_2 - k_3)\delta_{67}/\beta$, while the small stripes in the enhanced envelopes are influenced by rays 1, 6, and 7.

4. MEASUREMENT OF PARAMETERS

As mentioned above, the contour of the envelope in region B and the fringes in region C are influenced by rays 6, 7, and rays

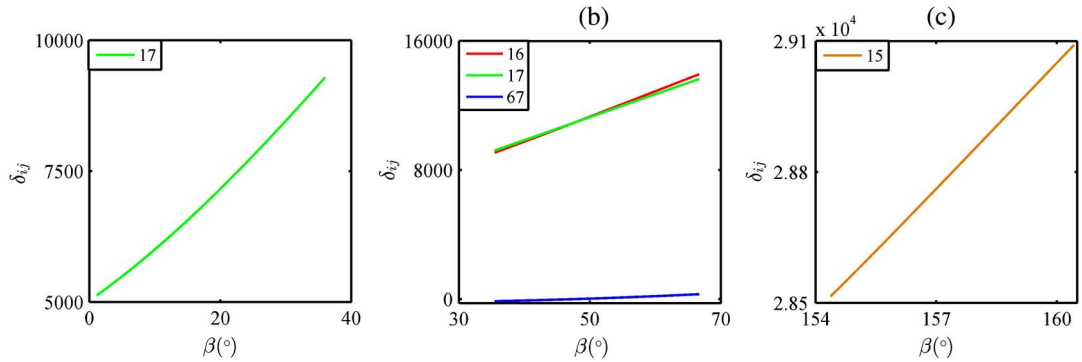

Fig. 7. Relationship between δ_{15}, δ_{16}, δ_{17}, δ_{67}, and β in regions: (a) A; (b) B; (c) C.

1, 5, respectively. Therefore, measurement of the angular width of the fringes can be used to obtain the parameters of the capillary and the liquid. To that end, the relation between the angular width and the parameters must be established. Angular widths of interference fringes in region C are related to n_0 and R, because rays 1 and 5 do not pass through the liquid inside the tube. Conversely, rays 6 and 7 go through the liquid, so the angular widths of envelopes in region B are not only well related to n_0 and R but also to n and r.

Before further derivation, a useful result is introduced first. Take ray 7 as an example. Based on Eqs. (1g) and (12), basic geometry, and the laws of refraction and reflection, we can derive

$$\frac{\partial L}{\partial \beta} = 2\left(R\sin\theta\frac{\partial\theta}{\partial\beta} - n_0 R\sin\frac{\partial\varphi}{\partial\beta} + n_0 r\sin\delta\frac{\partial\delta}{\partial\beta} - nr\sin\alpha\frac{\partial\alpha}{\partial\beta}\right)$$
$$= 2R\sin\theta\frac{\partial(\theta-\varphi+\delta-\alpha)}{\partial\beta} = R\sin\theta. \quad \textbf{(16)}$$

It is demonstrated for all the seven rays that the first-order partial derivatives of the optical path length L with respect to the deviation angle β have the same expression, i.e., $R\sin\theta$.

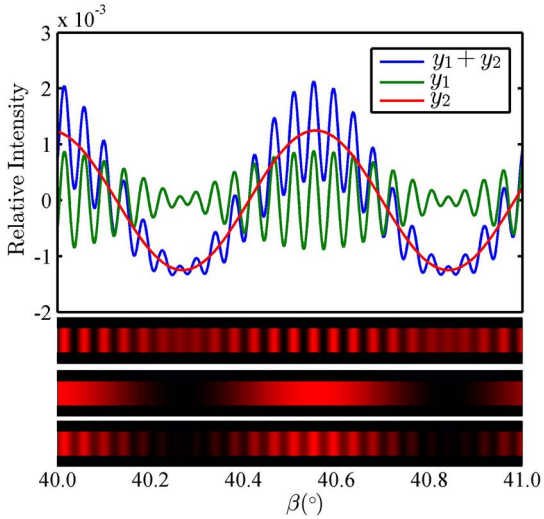

Fig. 8. Relationship between $y_i (i = 1, 2)$ and β in a range of 1 (°). (b), (c), and (d) are simulated results corresponding to y_1, y_2, and $y_1 + y_2$, respectively. The parameters are $n_0 = 1.4710$, $R = 0.505$ mm, $r = 0.256$ mm, and $n = 1.5323$.

This conclusion is determined by Fermat's principle [20,21] and the structure of the capillary, and it greatly simplifies the calculation of the parameters.

To determine the outer radius of the capillary and the RI of the wall material, we consider the interference fringes in the angular region C, which is drawn into a schematic diagram as in Fig. 9. Assuming β and $\beta + \Delta\beta$ are the deviation angles of the two adjacent bright fringes and the corresponding angular width of these two fringes is $\Delta\beta$. In this case, variation of optical path length difference between rays 1 and 5 is exactly one wavelength, i.e., $\Delta(\Delta L) = \lambda$ ($\Delta L = L_1 - L_5$). If ΔL and β are extremely small, $\Delta(\Delta L)$ can be approximated as follows:

$$\Delta(\Delta L) = \frac{d(\Delta L)}{d\beta}\Delta\beta = \left(\frac{dL_1}{d\beta} - \frac{dL_5}{d\beta}\right)\Delta\beta = \lambda. \quad \textbf{(17)}$$

Inserting Eq. (16) into Eq. (17), we have

$$\Delta\beta = \frac{\lambda}{R(\sin\theta_1 - \sin\theta_5)}. \quad \textbf{(18)}$$

According to Eq. (1e), we obtain

$$\beta_5 = 2\theta_5 - 4\arcsin\frac{\sin\theta_5}{n_0} + \pi, \qquad \arcsin\frac{rn_0}{R} \le \theta_5 \le \frac{\pi}{2}. \quad \textbf{(19)}$$

If rays 1, 5 interfere at the same spot of the screen, deviation angles of rays 1, 5 are the same, i.e., $\beta_1 = \beta_5 = \beta$. Measuring one group of $\Delta\beta$ and β of the fringes on the screen, and substituting β into Eq. (1a), we obtain $\theta(\theta_1)$. In Eqs. (18) and (19), θ_5, R, and n_0 are unknown, but the curve of the relation between n_0 and R can be obtained. Measuring several angular

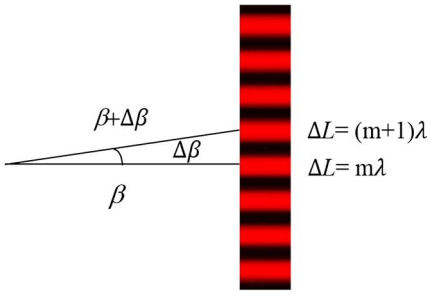

Fig. 9. Relationship between angular width and optical path differences.

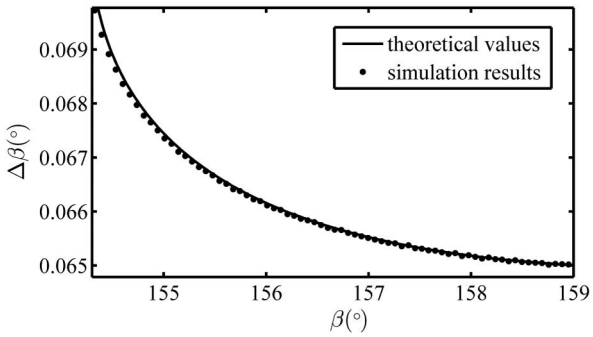

Fig. 10. Relationship between $\Delta\beta$ and β. The parameters are $n_0 = 1.4710$, $R = 0.505$ mm, $r = 0.256$ mm, and $n = 1.5323$.

widths at different deviation angles of fringes, we obtain several similar curves, and the values of their intersection are n_0 and R.

For the parameters of n and r, the same operations are performed by measuring the interference fringes in region B. Applying Snell's law to simplify Eqs. (1f) and (1g), we have

$$\beta_6 = 2\left(\theta_6 - \arcsin\frac{\sin\theta_6}{n_0}\right)\left[\arcsin\frac{rn_0}{R} \le \theta_6 \le \frac{\pi}{2}\right], \quad (20)$$

$$\beta_7 = 2\left(\theta_7 - \arcsin\frac{\sin\theta_7}{n_0} + \arcsin\frac{R\sin\theta_7}{rn_0} - \arcsin\frac{R\sin\theta_7}{rn}\right)\left[0 \le \theta_7 \le \arcsin\frac{rn_0}{R}\right]. \quad (21)$$

Similar to Eq. (18), we obtain

$$\Delta\beta = \frac{\lambda}{R(\sin\theta_6 - \sin\theta_7)}. \quad (22)$$

Measuring the deviation angles and angular widths of interference fringes in angular region B, several curves that show the relations between n and r are obtained, the values of their intersection are the required parameters. However, Eq. (17) has a mathematical approximation, the error caused by it must be analyzed. As an example, we consider the interference fringes in region C. Based on Eqs. (1a), (1e), and (18), the relationship between $\Delta\beta$ and β can be calculated. Meanwhile, we measure $\Delta\beta$ and β in simulated patterns. Results are shown in Fig. 10. Because the simulated results based on the ray tracing method are obtained without any approximation, we draw a conclusion from Fig. 10 that error caused by Eq. (17) is very small.

Therefore, we obtain four parameters of capillary and liquid by the following two steps: first, the RI of the wall n_0 and the outer radius R are determined by measuring the interference fringes in region C; second, RI of liquid n and the inner radius r are obtained by measuring interference fringes in region B. It is worth noting that only with Eq. (18) and Eq. (22) derived from Eq. (16), the derivation of the parameters can be simplified. There are three unknowns (n_0, θ_1, and θ_5) in Eqs. (1a) and (19), thus n_0 cannot be obtained, but by adding Eq. (18), one obtains the relation between n_0 and R. Similarly, n and r can be determined by adding Eq. (22). Therefore, Eq. (16) can greatly simplify the calculation of the parameters.

Further, to calculate the error of the method, a virtual experiment is built to measure four parameters. We measure angular widths of the simulated fringes (as listed in Table 2), and calculate the parameters by using the proposed method, the results are displayed in Table 3. Comparing the numerical results with the default value set in the simulation, it shows that the maximum error of the method is of 0.0001 order. Further, in the practical experiment, patterns are measured as listed in Table 4, and the results in Table 5 show the errors are of 0.001 order. It is primarily because of the inaccurate measurement of the fringe spacing. The accuracy of the charge-coupled device (CCD) light distribution instrument used in the practical experiment is 0.0005°, and the error caused by it is also of 0.001 order. If a more accurate instrument can be used to measure the fringe spacing, higher accuracy can be achieved.

Table 2. Deviation Angles and the Angular Widths of Interference Fringes in Regions C and B in Virtual Measurement[a]

	C						B					
β(°)	159.96	159.05	158.00	157.02	155.99	155.07	40.01	39.02	38.00	37.04	35.99	34.99
$\Delta\beta$(°)	0.0649	0.0650	0.0652	0.0655	0.0662	0.0673	0.6096	0.6256	0.6420	0.6577	0.6750	0.6917

[a] The parameters are $n_0 = 1.4710$, $R = 0.505$ mm, $r = 0.256$ mm, and $n = 1.5323$.

Table 3. Results Obtained by Using Our Method and Default Values

	R (mm)	n_0	r (mm)	n
numerical results	0.504889	1.47075	0.256047	1.53213
default values	0.505000	1.47100	0.256000	1.53230
inherent error (%)	0.022	0.017	0.018	0.011

Table 4. Deviation Angles and the Angular Widths of Interference Fringes in Regions C and B in Practical Measurement

	C						B					
β(°)	159.30	158.41	158.8685	158.64	157.10	156.26	52.53	50.81	50.42	49.94	48.84	45.28
$\Delta\beta$(°)	0.0651	0.0652	0.0651	0.0651	0.0657	0.0662	0.4394	0.4373	0.4579	0.4762	0.4826	0.5272

Table 5. Results Obtained by Using Our Method and Other Precise Methods

	R (mm)	n_0	r (mm)	n
experimental results	0.507	1.4650	0.257	1.5459
nominal value	0.505	1.471	0.256	1.5323
Error (%)	0.41	0.39	0.39	0.89

5. CONCLUSION

We have analyzed the patterns of a capillary filled with a liquid. Based on these analyses, a method is developed to measure the parameters of capillary and the liquid in it, and the error of this method is estimated to be of 0.0001 order. An experiment is built to measure the parameters with the method; the error is of 0.001 order; this is primarily because of inaccurate measurement of fringe spacing by a CCD light distribution instrument. Since our method is based on wave optics, it applies to a capillary as thin as a human hair. This method can also be used to measure the parameters of other transparent double-layer cylinders, such as optical fibers, biological tubes, and more.

Funding. National College Innovation Program of Beijing University of Posts and Telecommunications (BUPT); Fundamental Research Funds for the Central Universities.

Acknowledgment. The authors thank Zhibo Hou for discussions and suggestions.

REFERENCES

1. S. Calixto, M. Rosete-Aguilar, D. Monzon-Hernandez, and V. P. Minkovich, "Capillary refractometer integrated in a microfluidic configuration," Appl. Opt. **47**, 843–848 (2008).
2. Q. Li and X. Pu, "Measurement of the refractive index of microquantity liquid filled in a capillary and a capillary wall without destruction," Appl. Opt. **52**, 5318–5326 (2013).
3. Y. Xu, O. Sasaki, and T. Suzuki, "Double-grating interferometer for measurement of cylinder diameters," Appl. Opt. **43**, 537–541 (2004).
4. A. Yang, W. Li, G. Yuan, J. Dong, and J. Zhang, "Measuring the refractive indices of liquids with a capillary tube interferometer," Appl. Opt. **45**, 7993–7998 (2006).
5. H. S. Sørensen, H. Pranov, N. B. Larsen, D. J. Bornhop, and P. E. Andersen, "Absolute refractive index determination by microinterferometric backscatter detection," J. Anal. Chem. **75**, 1946–1953 (2003).
6. H. J. Tarigan, P. Neill, C. K. Kenmore, and D. J. Bornhop, "Capillary-scale refractive index detection by interferometric backscatter," J. Anal. Chem. **68**, 1762–1770 (1996).
7. K. Swinney, D. Markov, and D. J. Bornhop, "Chip-scale universal detection based on backscatter interferometry," J. Anal. Chem. **72**, 2690–2695 (2000).
8. H. Zhu, I. M. White, J. D. Suter, M. Zourob, and X. Fan, "Integrated refractive index optical ring resonator detector for capillary electrophoresis," J. Anal. Chem. **79**, 930–937 (2007).
9. C. K. Kenmore, S. R. Erskine, and D. J. Bornhop, "Refractive-index detection by interferometric backscatter in packed-capillary high-performance liquid chromatography," J. Chromatogr. A **762**, 219–225 (1997).
10. S. Qi, Y. Liu, X. Yang, T. Xu, G. Chen, C. Zhang, and J. Tian, "Measurement of nonlinear refractive index of ethyl red by interference of capillary," Opt. Commun. **281**, 5902–5904 (2008).
11. H. El Ghandoor, E. Hegazi, I. Nasser, and G. Behery, "Measuring the refractive index of crude oil using a capillary tube interferometer," Opt. Laser Technol. **35**, 361–367 (2003).
12. P. Grosso, D. Malardé, M. Le Menn, and Z. Wu, "Refractometer resolution limits for measuring seawater refractive index," Opt. Eng. **49**, 103603 (2010).
13. Z. Hou, X. Zhao, and J. Xiao, "A simple double-source model for interference of capillaries," Eur. J. Phys. **33**, 199 (2012).
14. Z. You, D. Jiang, J. Stamnes, J. Chen, and J. Xiao, "Characteristics and applications of two-dimensional light scattering by cylindrical tubes based on ray tracing," Appl. Opt. **51**, 8341–8349 (2012).
15. Z. You, D. Jiang, Z. Hou, and J. Xiao, "Analysis of light scattered by a capillary to measure a liquid's index of refraction," Am. J. Phys. **80**, 688–693 (2012).
16. B. Krattiger, A. E. Bruno, H. M. Widmer, M. Geiser, and R. Dändliker, "Laser-based refractive-index detection for capillary electrophoresis: ray-tracing interference theory," Appl. Opt. **32**, 956–965 (1993).
17. Y. Qin, A. Michalowski, R. Weber, S. Yang, T. Graf, and X. Ni, "Comparison between ray-tracing and physical optics for the computation of light absorption in capillaries–the influence of diffraction and interference," Opt. Express **20**, 26606–26617 (2012).
18. Y. Takano and M. Tanaka, "Phase matrix and cross sections for single scattering by circular cylinders: a comparison of ray optics and wave theory," Appl. Opt. **19**, 2781–2800 (1980).
19. E. Hecht, *Optics*, 4th ed. (Addison Wesley Longman, 1998).
20. R. Schlegel, "Optical refraction and Fermat's principle at a point," J. Opt. Soc. Am. **40**, 244–245 (1950).
21. M. Se-yuen, "A closer look at Fermat's principle," Phys. Educ. **21**, 365 (1986).